Digest Journal of Nanomaterials and Biostructures Vol. 19, No. 1, January - March 2024, p. 417 - 433

Investigation on spinnability of low molecular weight alkaline lignin to fabricate biobased carbon fiber

C. Shen, J. Li, D. Guo, L. Sha, J. Li*
School of Environmental and Natural Resources, Zhejiang University of Science & Technology, Hangzhou 310023, Zhejiang, China

Using acetic acid instead of dimethylformamide as solvent, lignin-based nanofibers were prepared by electrospinning with industrial low molecular weight lignin. After pre-oxidation and carbonization, the fibril was transformed into carbon fiber. The results showed that different viscosity of spinning solution and different parameters of electrospinning have great influence on the morphology of fibers. The diameter of fibers could be concentrated in 300-500nm by using the best electrospinning process. After carbonizing the fibers, it was found that the lignin fibers could retain the morphology of the fibers after carbonization at a suitable heating rate and holding temperature. This study showed the conditions required for the preparation of carbon fiber from low molecular weight lignin, and provided a way for high value utilization of waste biomass and green preparation of carbon fiber.

(Received January 10, 2024; Accepted March 13, 2024)

Keywords: Lignin, Carbon fibers, Low molecular weight, Electrospinning

1. Introduction

Carbon fiber was an important material in industry today because of its high tensile strength, high stiffness, chemical resistance, high temperature resistance, low weight and low thermal expansion. It has been widely used in transportation, construction, aerospace, life and health[1-4], new energy and other fields. In the trend of increasing demand for it, carbon fiber prepared from polyacrylonitrile (PAN) has the disadvantages of high cost and non-degradation. The solvent dimethylformamide (DMF) is also highly volatile and toxic, which has a bad effect on the surrounding environment during the preparation process. Therefore, the use of biodegradable materials to produce carbon fiber has become a current research hotspot. Lignin, with its high carbon content and biodegradability, is a good substitute for PAN[5]. Its application is limited mainly because of its amorphous chemical structure, low molecular weight, wide molecular weight distribution and poor arrangement[6-9]. If carbon fiber can be prepared from lignin, the development of green raw materials of carbon fiber and high value utilization of lignin can be completed at the same time[10, 11].

Nowadays, many researches have succeeded in making lignin spinnable by increasing the molecular weight of lignin. Shi et al[12]. designed a method for classifying lignin, and treated corn stalks in different solutions and temperatures for a total of more than 50 hours to obtain lignin with high molecular weight (Mw: 6966) and linear molecular structure, and prepared carbon fibers with excellent properties from this lignin. Zhu et al[13]. used dialysis bags with molecular weights of 3.5K and 7K to dialysis the modified lignin solution, and separated three components of 3.5K, 3.5K-7K, and 7K. The molecular weight of lignin was increased and the heterogeneity of lignin was reduced. The carbon nanofibers prepared from lignin were smooth and the average diameter was about 390nm. Jin et al.[14] fully mixed raw lignin with acetic acid aqueous solution and placed it for 30 seconds. The mixture was separated into two liquid phases. The liquid phase with more

* Corresponding author: 779892031@qq.com
https://doi.org/10.15251/DJNB.2024.191.417

solvents contained a lot of metal salts/impurities and low molecular weight lignin, while the liquid phase with more lignin contained purified high molecular weight lignin, and the high molecular weight lignin was obtained by this method. Li et al.[15] developed an enzyme medium system for the fractionation of lignin. The lignin after fractionation is a high-quality carbon fiber precursor with large molecular weight and few functional groups, and can prepare carbon nanofibers with excellent properties. It is found that most of the current studies on the preparation of lignin based fibers refer to increasing the molecular weight of lignin to make it easier to spin. But in fact, using dialysis, filtration and other methods to purify lignin takes a lot of time and a lot of additives. The use of enzymes or precision dialysis tubes and other methods require a large cost, the market of high molecular weight lignin is expensive. In addition, the above method of optimizing the molecular weight of lignin is too complicated to be applied to industry and difficult to scale up.

In this study，the viscosity of lignin spinning solution was improved by using PEO as spinning aid, and the spinnability of the spinning solution was greatly improved.By exploring the effects of different process parameters on the preparation of spinning solution, electrospinning and carbonization, an optimal process condition was found for the preparation of carbon fiber from low molecular weight lignin produced by industry. It has broad application prospects in paper industry, lignin waste and lignocellulosic biorefinery and provides a way for the preparation of lignin based biorenewable carbon fiber.

2. Experimental

2.1. Materials

Alkaline lignin (AL, average MW = 505.01) was supplied by Qiyue Biology Co., Ltd. (Xian, China). Polyethylene oxide (PEO, MW = 200000), acetic acid were purchased from Macklin. All the chemicals and solvents were used without further purification.

2.2. Preparation of spinning solution

First, the appropriate amount of lignin and the corresponding proportion of PEO were dissolved in acetic acid and dissolved in a magnetic stirrer at 90 oC and 500 r/min for 60 min to obtain a preliminary mixed solution. Then, the solution was transferred to an electric mixer, dissolved at 75 oC and 500 r/min for 1 h, and ultrasonically dispersed for 30 min. By the above method, Lignin /PEO mixed solutions with solid mass fractions of 15, 20, 25 and 30 wt.% were prepared in which the added amounts of PEO were 1 wt.%, 3 wt.%, 5 wt.% and 10 wt.% (w/w, relative to lignin mass).

2.3 Electrospinning

Based on the experimental results, the optimal electrospinning effect was achieved when the viscosity ranged from 350 mPa·s to 450 mPa·s. Therefore, the spinning solution with a total mass fraction of 25% for lignin and PEO in a ratio of 95:5 and a stirring time of 1 hour was selected for electrospinning. The electrospinning setup consisted of a high-voltage power supply, a syringe pump, a needle, a collector, and a slide. The high-voltage power supply regulated the positive and negative voltages, the syringe pump controlled the flow rate of the spinning solution, and the slide controlled the speed and distance of the needle movement. Electrospinning was carried out in a horizontal orientation using a 5 mL syringe fitted with a 20G sized needle as a spinneret connected to the positive terminal of a high voltage power supply. The operating voltage was 18~24 kV and the collecting distance was 10~20 cm. An aluminum foil sheet was used as the collector and was connected to ground. A syringe pump operating at a feed rate of 0.6~1.2 mL/min supplied the polymer solution to the spinneret. Under the aforementioned electrospinning conditions, lignin-based nanofiber membranes were obtained, dried in a vacuum at 60°C for 1 hour and peeled off from the aluminum foil for further use.

2.4 Oxidative thermal stabilization and carbonization

The spun fibers were placed in a tubular furnace and pre-oxidized at temperatures of 200°C, 220°C, 250°C, and 270°C in air with a heating rate of 0.4°C/min and held isothermally for

60 min. Subsequently, Samples were heated to 500, 600, or 700 °C with a heating rate 3°C/min and held isothermally at the selected carbonization temperature for different times 30min, 60min, 90min.

2.5. Characterization

2.5.1. Structural properties

Potassium bromide was ground into a uniform powder in an agate mortar and then pressed into a transparent sheet using a pellet press. The sample was evenly coated on the sheet and analyzed using a Fourier-transform infrared spectrometer. The wavelength scan range was 4000~400 cm-1, with 32 scans and a resolution of 4 cm-1.

2.5.2. Thermal properties

The sample was placed in a thermogravimetric analyzer, and the instrument was heated from room temperature to 800°C at a constant nitrogen flow rate of 100 mL/min and a heating rate of 10°C/min to evaluate the thermal stability of the sample.

2.5.3. Viscosity properties

The spinning solution was filled into a 50 mL bottle, and a digital viscometer was used to measure the viscosity of the spinning solution using 1, 2, 3, or 4 rotor numbers, depending on the viscosity range of the spinning solution.

2.5.4. Morphology

The surface morphology of the fibers electrospun under different conditions was observed using a scanning electron microscope. Image analysis software (Image-Pro) was used to measure the fiber diameter in the electron microscope images (50 fibers were selected from each sample).

3. Results and discussion

3.1. Spinning solution

3.1.1. Fourier-Transform Infrared Spectroscopy (FT-IR) and viscosity of the Spinning Solution

FTIR spectra of all precursors are given in Figure 1 (a)(b)(c)(d). From the spectrum, stretching vibrations of -OH, -CH2, and C-O-C bonds were observed at 3450 cm-1, 2926 cm-1, and 1285 cm-1, respectively. The absorption peaks at 1628 cm-1 and 1563 cm-1 were related to the stretching vibrations of the -C=C- bond in benzene. The absorption peak at 835 cm-1 was attributed to the C–H rocking vibration absorption peak of PEO. The absorption peak at 625 cm-1 indicated the aliphatic C–C stretching vibration.The four spectra indicate that changes in stirring time, mass fraction, and the mixture ratio of lignin and PEO did not result in the appearance of new absorption peaks or the disappearance of existing ones. Therefore, altering the preparation conditions of the spinning solution within this range does not affect its basic chemical properties.

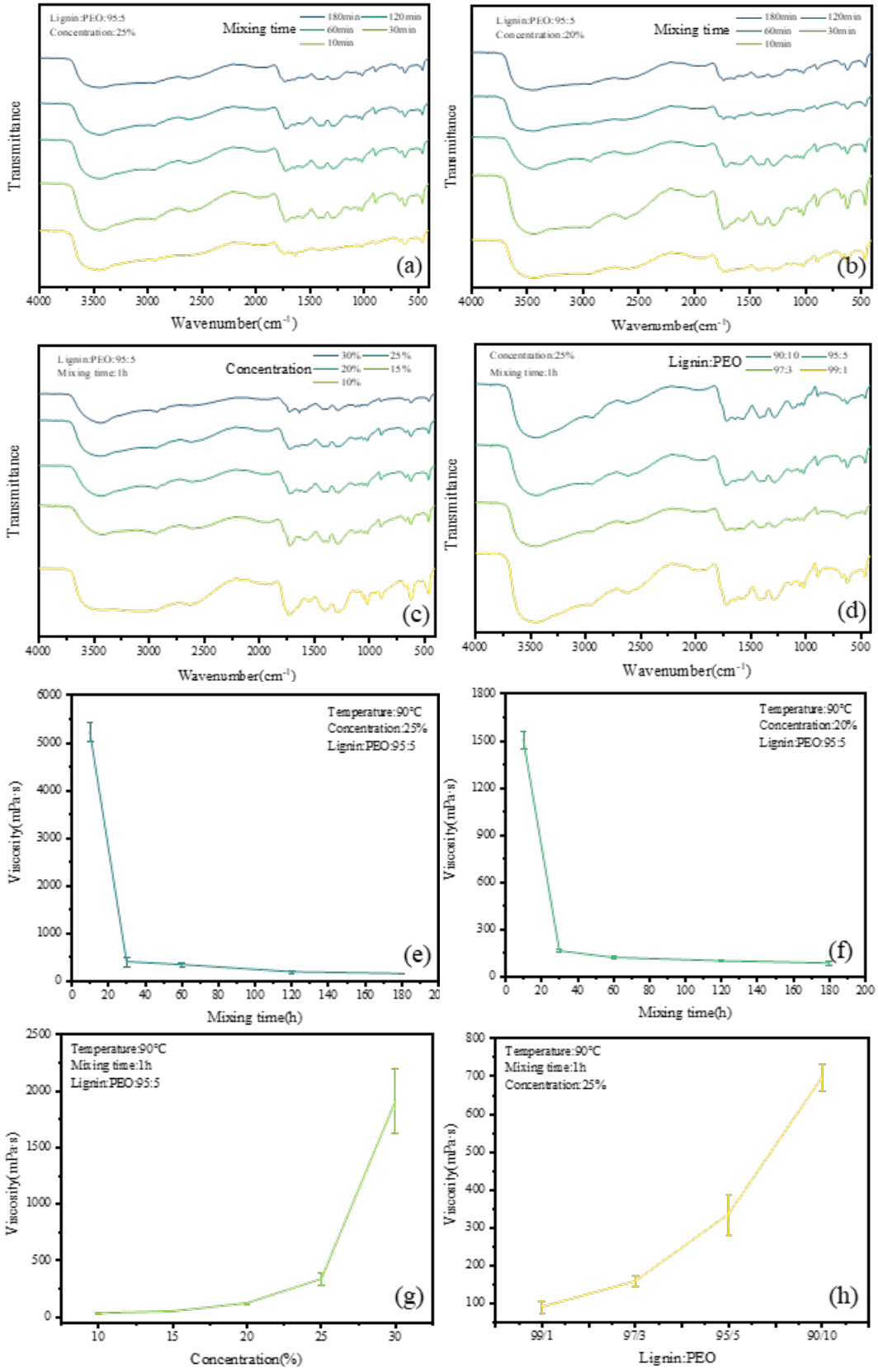

Fig. 1. FT -IR spectra of spinning solution produced from various stirring times, lignin contents and Lignin to PEO ratios (a) Stirring time (the lignin content was 25wt%), (b) Stirring time (the lignin content was 20wt%), (c) Lignin content (d) Lignin to PEO ratio, and viscosity change of spinning solution with different (e) stirring time (lignin content 25wt%), (f) stirring time (lignin content 20wt%), (g) lignin content, and (h) lignin to PEO ratio.

Table 1. The assignment of FTIR absorption peak of spinning solution.

Wavenumber, cm^{-1}	Absorption peak
3450	Vibration absorption peak of intermolecular H-bonding
2926	The $-CH_2$ vibration absorption peak
1628	The -C=C- Vibration absorption peak on benzene ring
1563	The -C=C- Vibration absorption peak on benzene ring
1285	The C–O–C stretching vibration absorption peak of PEO
835	The C–H rocking vibration absorption peak of PEO
615	The aliphatic C–C stretching vibration

The rheological properties of the spinning solution, particularly its viscosity, are closely related to the success of the spinning process. When the viscosity is too low, the needle will drip and make the jet unstable, and the diameter of the jet will shrink under the action of surface tension, resulting in beading between the fibers. If the viscosity is too high, it is difficult to form a liquid jet, which will affect the electrospinning process. The viscosity of the spinning solution is influenced by various factors. In this study, the effects of lignin mass fraction, stirring time of the spinning solution, and the addition of polyethylene oxide (PEO) on viscosity were investigated, and a set of parameters suitable for electrospinning was determined.

Viscosity characterization was performed on the spinning solution. As shown in Figure 1 (e) and (f), it can be observed that the initial viscosity of the spinning solution increased by approximately 3.5 times when the lignin mass fraction increased from 20% to 25%. This result is inconsistent with some literature reports, which may be attributed to the fact that in those studies, lignin was used as an auxiliary material with a lower addition amount and almost no change in mass fraction. In such cases, the addition of lignin would decrease the viscosity of the solution. However, in this study, lignin was used as the main raw material, and the mass fraction of the spinning solution increased significantly along with the lignin content, resulting in an increase in viscosity instead of a decrease. After stirring for 30 minutes, the viscosity of the spinning solution with a mass fraction of 25% dropped sharply and was approximately twice that of the spinning solution with a mass fraction of 20%. The viscosity continued to decrease with an increase in stirring time, but the rate of decrease became smaller. After stirring for 120 minutes, the viscosity reached a plateau and remained almost unchanged. After stirring for 180 minutes, the viscosity of the latter sample was approximately 1.5 times that of the former sample.

Figure 1 (g) shows that the viscosity of the spinning solution gradually increased with an increase in the lignin mass fraction, and the rate of increase became larger. The viscosity increased by about 5 times from 25% to 30% mass fraction. This may be due to the fact that the solubility of lignin in acetic acid is close to its limit at a mass fraction of around 30%. The sample with a mass fraction of 30% also exhibited solidification after cooling and standing, which would cause needle blockage during spinning. In contrast, the influence of the ratio of lignin to PEO on the viscosity of the spinning solution, as shown in Figure.1 (h), was relatively weak. Therefore, the viscosity of the spinning solution can be finely adjusted by adjusting the ratio of lignin to PEO.

After electrospinning the aforementioned spinning solution, the best electrospinning effect was achieved when the viscosity of the spinning solution was within the range of 350 mPa·s to 450 mPa·s. A viscosity that is too low can cause dripping from the needle, while a viscosity that is too high can lead to needle blockage. Both phenomena prevent the formation of a stable Taylor cone and hinder the spinning process.

3.1.2. Thermal Characterization of the Spinning Solution

Thermal gravimetric analysis (TGA) was performed on the spinning solution. Figure 2 (a) show the TGA and differential thermogravimetric analysis (DTGA) curves of the spinning solution under different stirring times, while Figure.2 (b) show the TGA and DTGA curves of the spinning

solution with different viscosities. Five thermal degradation stages were observed. The first stage occurred between 100°C and 200°C, and the weight loss in this stage was mainly attributed to the evaporation of residual acetic acid and water in the sample. The second stage occurred between 200°C and 250°C, with a relatively small weight loss, which was caused by the degradation of PEO. The last three stages occurred between 270°C and 320°C, 380°C and 410°C, and 430°C and 490°C, respectively. The weight loss in these stages was related to the breakage of lignin molecular chains and the thermal cracking of the aromatic main chain. Differences in the first stage may be observed among samples with different stirring times or viscosities (e.g., samples with a viscosity of 1710 mPa·s and stirring times of 30 min and 120 min). This could be attributed to the strong water absorption of the samples, resulting in different initial water contents during TGA analysis. However, these water contents will completely evaporate during the spinning process and have no impact. In the last four stages, the thermal decomposition temperatures remained nearly constant under different conditions. In the fifth stage, the sample with a stirring time of 60 min and a viscosity of 296.6 mPa·s exhibited a 5°C to 10°C higher maximum degradation temperature compared to samples in the same group.

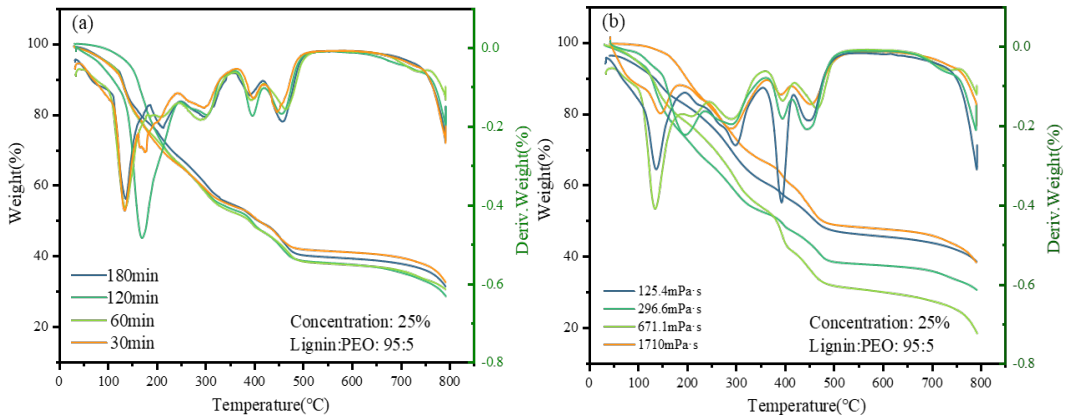

Fig. 2. Thermal decomposition of Spinning solution under different (a) mixing time, (b) viscosity (Lignin content: 25% Lignin to PEO ratio: 95:5).

3.2. Lignin-Based Nanofibers

3.2.1. Effect of Electrospinning Voltage on the Electrospinning Results

SEM images of the precursor fibers are shown in Figure 3. When the spinning voltage is 18kV, the fiber thickness difference is obvious, there are more disorderly fibers, and a large number of beads and condensation phenomenon, which may be due to the insufficient electric field force generated by the small voltage, and the instability of Taylor cone. At the same time, the fiber is not sufficiently stretched under the action of small electric field forces, resulting in the fiber diameter concentrated between 300 and 700nm. When the voltage is 20kV, the fiber diameter is uniform, the disorderly fiber is less, the fiber fracture and beads are less, and the fiber diameter is concentrated in 300~500nm. It may be that at a voltage of 20kV, the electric field is stable and the Taylor cone is relatively stable. When the voltage is increased to 22kV, the fracture sites are significantly increased, and the beading phenomenon is more serious. Meanwhile, there are more chaotic fibers than when the voltage is applied to 18kV, and the fiber diameter is smaller but not concentrated. Under 24kV voltage, the electric field force is large, and the tensile effect on the fibers is strong, resulting in the diameter of most of the fibers is small, and the fracture phenomenon is also very obvious. At high voltage, the electric field is not stable enough, resulting in serious beading phenomenon. In general, stable Taylor cone is a necessary condition for spinning fibers with uniform diameter and less broken beads, and the spinning voltage plays a key role in the stability of Taylor cone. Therefore, 20kV was selected as the best spinning voltage.

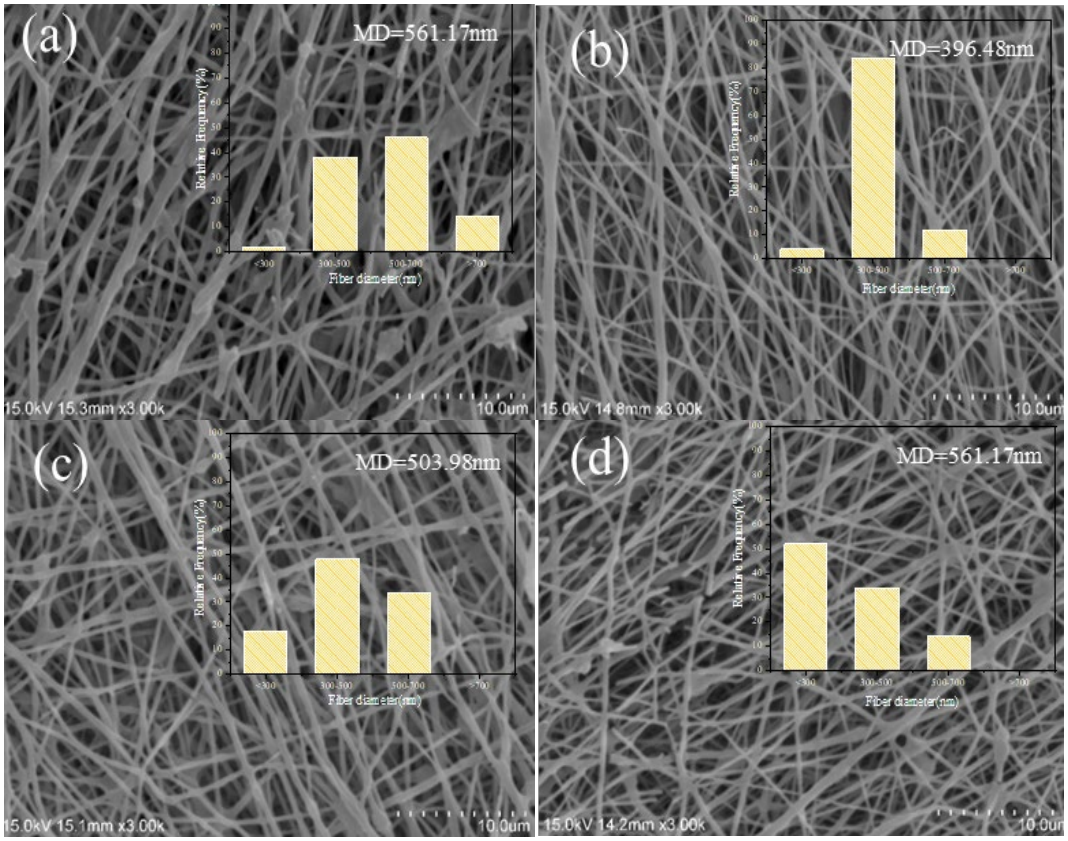

Fig. 3. SEM images and diameter distribution images of fibers at different spinning voltages: (a) 18kV, (b) 20kV, (c) 22kV, (d) 24kV; Note: feed rate 1.0 mL/h, collector distance 15 cm, roller speed 400 rpm.

3.2.2. Effect of Spinning Flow Rate on Electrospinning Results

Figure 4 shows when the spinning flow rate was 0.6 mL/h and 0.8 mL/h, there were more beads on the fibers, and their diameters were mainly distributed between 300 nm and 700 nm. The presence of more beads and a more chaotic arrangement of fibers were observed at a flow rate of 0.6 mL/h. This may be due to the slow flow rate, which resulted in a mismatch between the extrusion speed of the spinning solution and its consumption, leading to unstable Taylor cones. As a result, the diameter distribution of the fibers was not concentrated, and there was adhesion between the fibers. However, at a flow rate of 1.0 mL/h, there was almost no adhesion between the fibers, and the diameter distribution was more uniform. When the flow rate increased to 1.2 mL/h, the overall diameter of the fibers increased, and there were a large number of fibers with diameters larger than 700 nm, as well as more apparent adhesion. This may be due to the increase in flow rate, which resulted in less stretching of the spinning solution due to the electric field force per unit volume, leading to an increase in fiber diameter. In addition, the higher flow rate may have caused insufficient solvent evaporation, resulting in fiber adhesion. Therefore, a flow rate of 1.0 mL/h was chosen as the optimal spinning flow rate.

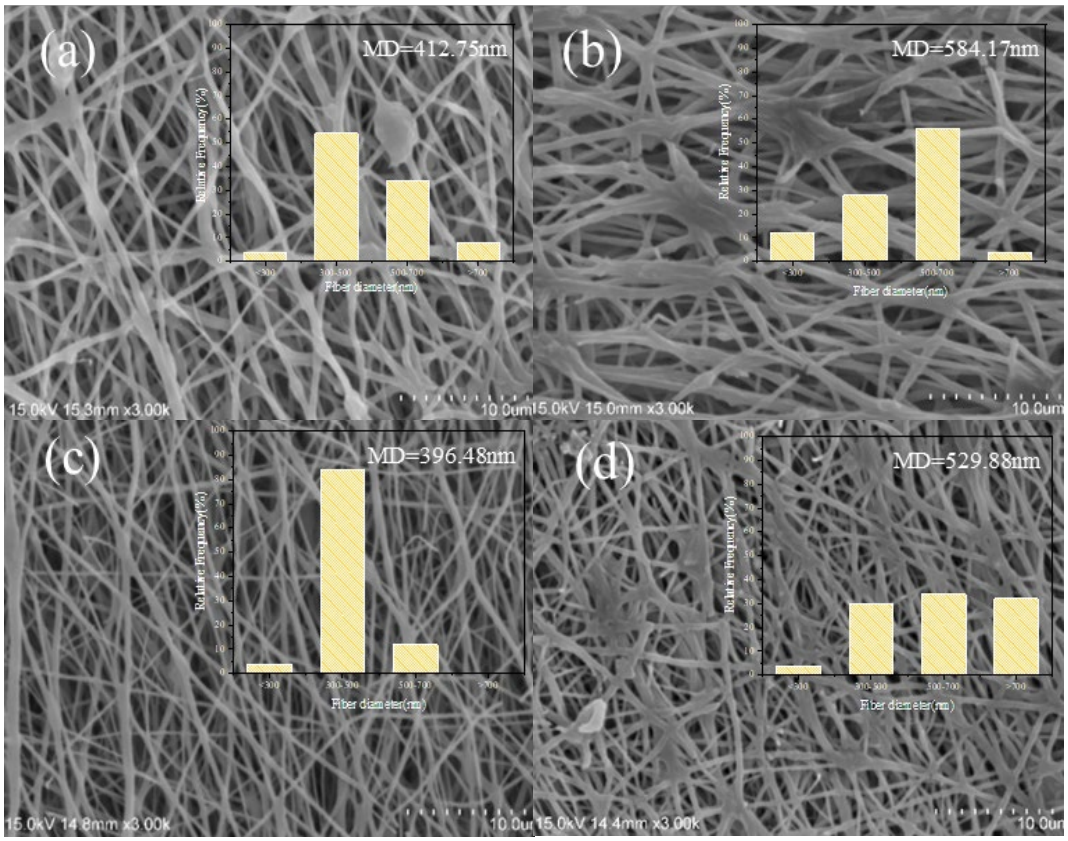

Fig. 4. SEM images and diameter distribution images of fibers at different feed rate: (a) 0.6mL/h, (b) 0.8mL/h, (c) 1.0mL/h, (d) 1.2mL/h; Note: Spinning voltage 20kV, collector distance 15 cm, roller speed 400 rpm.

3.2.3. Effect of Collector Distance on Electrospinning Results

Figure 4 shows when the spinning flow rate was 0.6 mL/h and 0.8 mL/h, there were more beads on the fibers, and their diameters were mainly distributed between 300 nm and 700 nm. The presence of more beads and a more chaotic arrangement of fibers were observed at a flow rate of 0.6 mL/h. This may be due to the slow flow rate, which resulted in a mismatch between the extrusion speed of the spinning solution and its consumption, leading to unstable Taylor cones. As a result, the diameter distribution of the fibers was not concentrated, and there was adhesion between the fibers. However, at a flow rate of 1.0 mL/h, there was almost no adhesion between the fibers, and the diameter distribution was more uniform. When the flow rate increased to 1.2 mL/h, the overall diameter of the fibers increased, and there were a large number of fibers with diameters larger than 700 nm, as well as more apparent adhesion. This may be due to the increase in flow rate, which resulted in less stretching of the spinning solution due to the electric field force per unit volume, leading to an increase in fiber diameter. In addition, the higher flow rate may have caused insufficient solvent evaporation, resulting in fiber adhesion. Therefore, a flow rate of 1.0 mL/h was chosen as the optimal spinning flow rate.

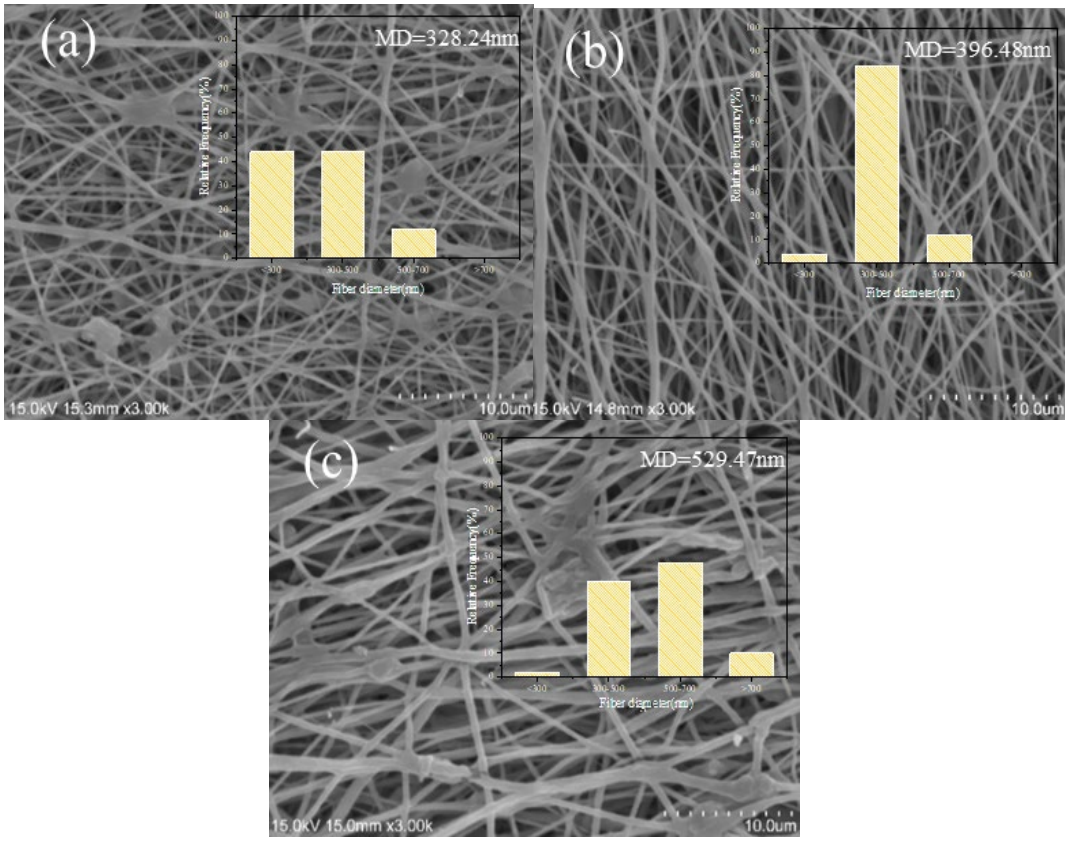

Fig. 5. SEM images and diameter distribution images of fibers at different receiving distances: (a) 10cm, (b) 15cm, (c) 20cm; Note: Spinning voltage 20kV, feed rate 1.0 mL/h, roller speed 400 rpm.

Based on Figure.5, it can be observed that when the collector distance was 10 cm, the fibers exhibited a chaotic orientation and a higher number of beads. This may be due to the unstable electric field caused by the short distance between the roller and the needle, resulting in random fiber orientation and increased bead formation. The close distance also prevented complete solvent evaporation, leading to severe fiber adhesion. Additionally, the shorter collector distance resulted in a higher electric field intensity for the same applied voltage on the needle, leading to stronger stretching of the fibers. As a result, most of the fibers had smaller diameters, primarily distributed below 500 nm, while the few fibers with larger diameters were caused by the unstable electric field. When the collector distance was 20 cm, the fibers had generally larger diameters and exhibited small-scale aggregation. This may be due to the reduced effect of electric field force on fiber stretching as the collector distance increased, causing the fibers to intertwine and form aggregates during the process of being sprayed onto the collector. However, at a collector distance of 15 cm, the fibers showed good orientation, a uniform diameter, and almost no aggregation or bead formation. Therefore, a collector distance of 15 cm was chosen as the optimal distance.

3.2.4. Effect of Roller Speed on Electrospinning Results

Figure 6 shows when the roller speed was 200 rad/min, the fiber diameter was large, with over 80% of the fibers having diameters larger than 500 nm. There was also a noticeable aggregation of fibers. This may be attributed to the low stretching effect on the fibers due to the low roller speed when the fibers landed on the roller. As a result, the fibers did not receive sufficient stretching and adhered to neighboring fibers. This indicates that a roller speed of 200 rad/min is too low. On the other hand, at a roller speed of 600 rad/min, the fiber diameter was uniform, with most fibers being small in diameter. However, there was severe fiber breakage. The high speed caused excessive stretching of the fibers, resulting in multiple breaks and the inability to form continuous fibers. In comparison, at a roller speed of 400 rad/min, there was less fiber

breakage and a uniform diameter. Therefore, a roller speed of 400 rad/min was chosen as the optimal speed.

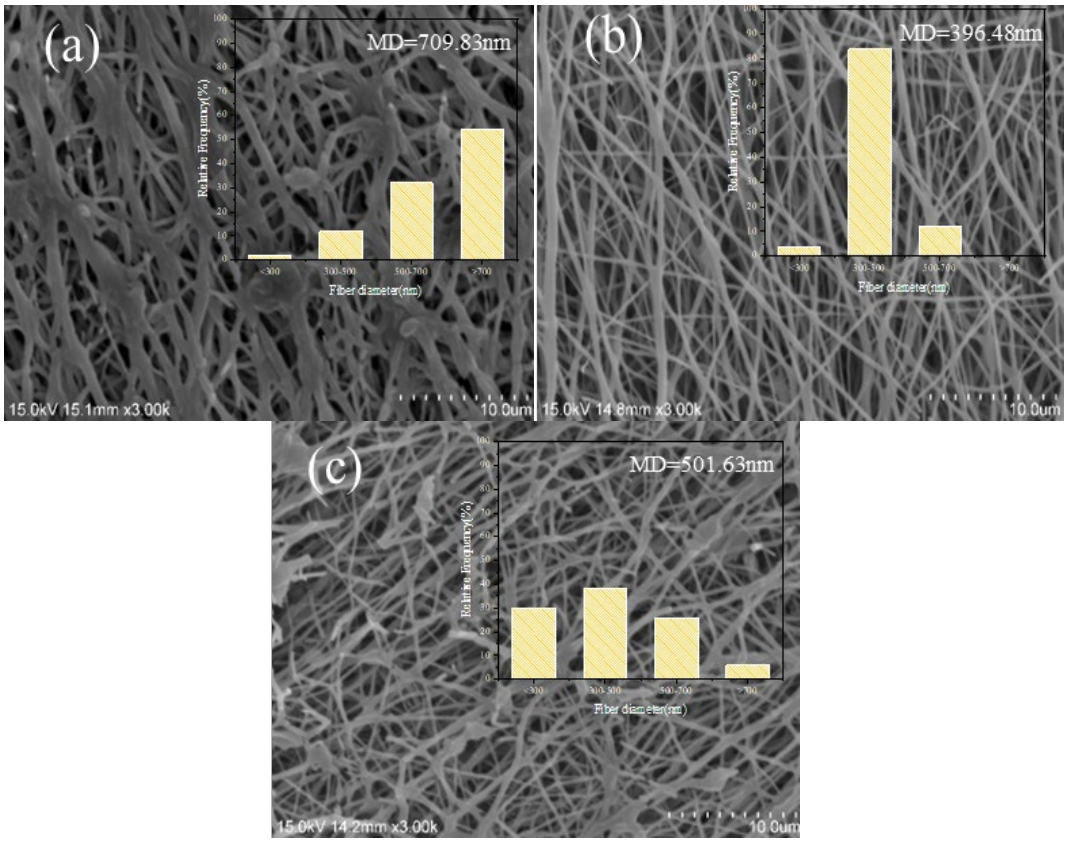

Fig. 6. SEM images and diameter distribution images of fibers at different roller speeds: (a) 200rad/min, (b) 400rad/min, (c) 600rad/min; Note: Spinning voltage 20kV, feed rate 1.0 mL/h, collector distance 15 cm.

3.2.5. Thermal Characterization of the Fibers

Figure 7 (a) displays the component with a flow rate of 1.0 mL/h had the lowest thermal decomposition weight loss. This may be attributed to the fact that fibers from this component had fewer beads, less breakage, and less adhesion, resulting in a more stable fiber structure. (b) shows that fibers produced at a voltage of 20kV had the lowest thermal decomposition weight loss, while fibers produced at 24kV had the highest. This may be due to the small diameter and severe breakage of the fibers. Fibers with a smaller diameter are more prone to breakage when heated, and the broken sections are more likely to undergo melting, leading to a rapid increase in the melting area.

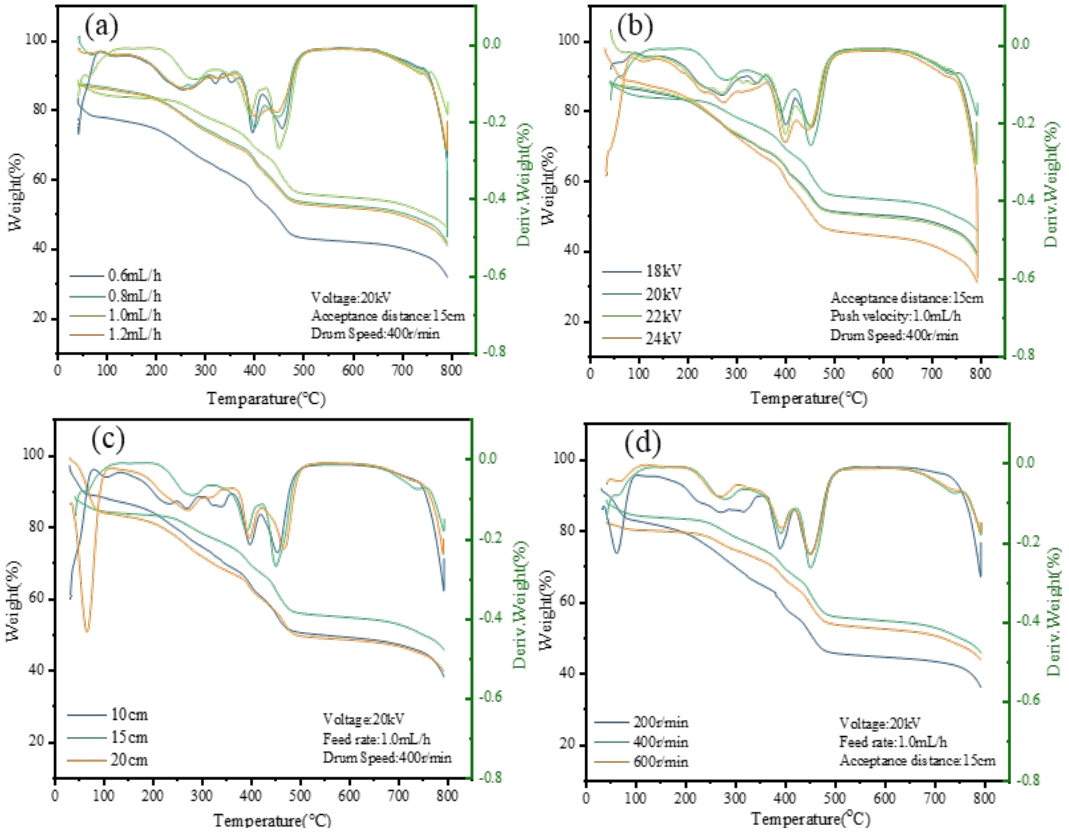

Fig. 7. Thermal decomposition of fibers prepared at different (a) feed rates, (b) spinning voltages, (c) acceptance distances, (d) drum speeds.

The thermal decomposition weight loss of fibers at a collector distance of 10 cm and 20 cm was almost the same in (c), and both were lower than that of the component at a distance of 15 cm. This may be attributed to the higher presence of beads in the components at distances of 10 cm and 20 cm. The beads are more likely to undergo melting during heating and then spread to the fibers, causing damage to the fiber structure. And (d) shows that the thermal decomposition weight loss of the component at 200 r/min is significantly higher than the other two groups. This indicates severe fiber aggregation and adhesion at a roller speed of 200 r/min, and such fiber structures cannot maintain their original structure during heating, resulting in a rapid expansion of the melting area.

Based on the DTG in (a)(b)(c)(d), it can be observed that changes in flow rate, voltage, collector distance, and roller speed have a minimal effect on the fiber thermal decomposition temperature. The thermal decomposition rate reaches its maximum between 390°C and 450°C.

In conclusion, the fiber structure has a significant influence on its stability during heating, and phenomena such as bead formation, breakage, aggregation, and adhesion are not favorable for maintaining the original fiber structure during heating. Therefore, the optimal parameters for fiber preparation for pre-oxidation and carbonization are a spinning voltage of 20kV, a flow rate of 1.0 mL/h, a collector distance of 15 cm, and a roller speed of 400 r/min.

3.2.6. Thermal Characterization of Pre-oxidized Fibers

In Figure 8, it can be seen that the sample with a preoxidation temperature of 200℃ decomposed faster at around 470℃ than other samples. At around 390℃, samples with a pre-oxidation temperature of 250℃ decompose faster. This may be caused by the difference in the number of molecular chains and aromatic rings of lignin in different samples. After 500℃, most of the impurities are burned, and the margin of all samples is almost the same, which also indicates

that the preoxidation has no great impact on the thermal properties of the fibers, and the preoxidation mainly plays a role in fixing the morphology of the fibers.

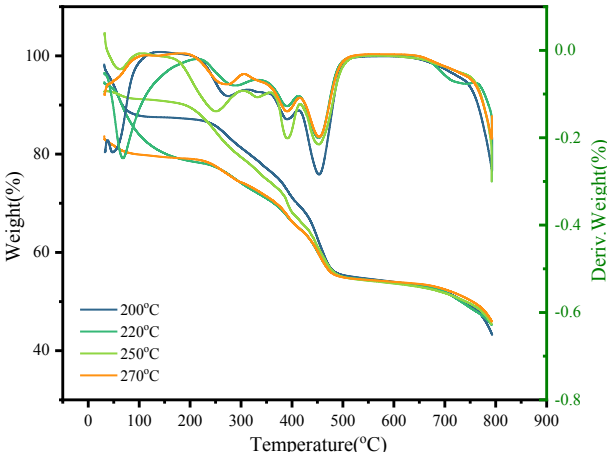

Fig. 8. Thermal decomposition of preoxidized fibers at different preoxidation temperatures.

3.3. Lignin-Based carbon Nanofibers

3.3.1. Thermal Characterization of carbon Fibers

In Figure 9, it can be seen that the carbonization holding time and pre-oxidation temperature have only minor effects on the thermal properties of carbon fibers. However, carbonization temperature has a certain effect on the thermal properties of carbon fiber. When the carbonization temperature is 700℃, the sample quality is almost not reduced, and the carbonization temperature of 500℃ and 600℃ samples will still decompose after the temperature reaches 650℃. This may be because the composition and morphology of the sample with a carbonization temperature of 700℃ are different from those of the other two groups (as can be obtained from Figure 11). When the carbonization temperature is increased to 700℃, the sample has become a completely molten state without any fiber morphology.

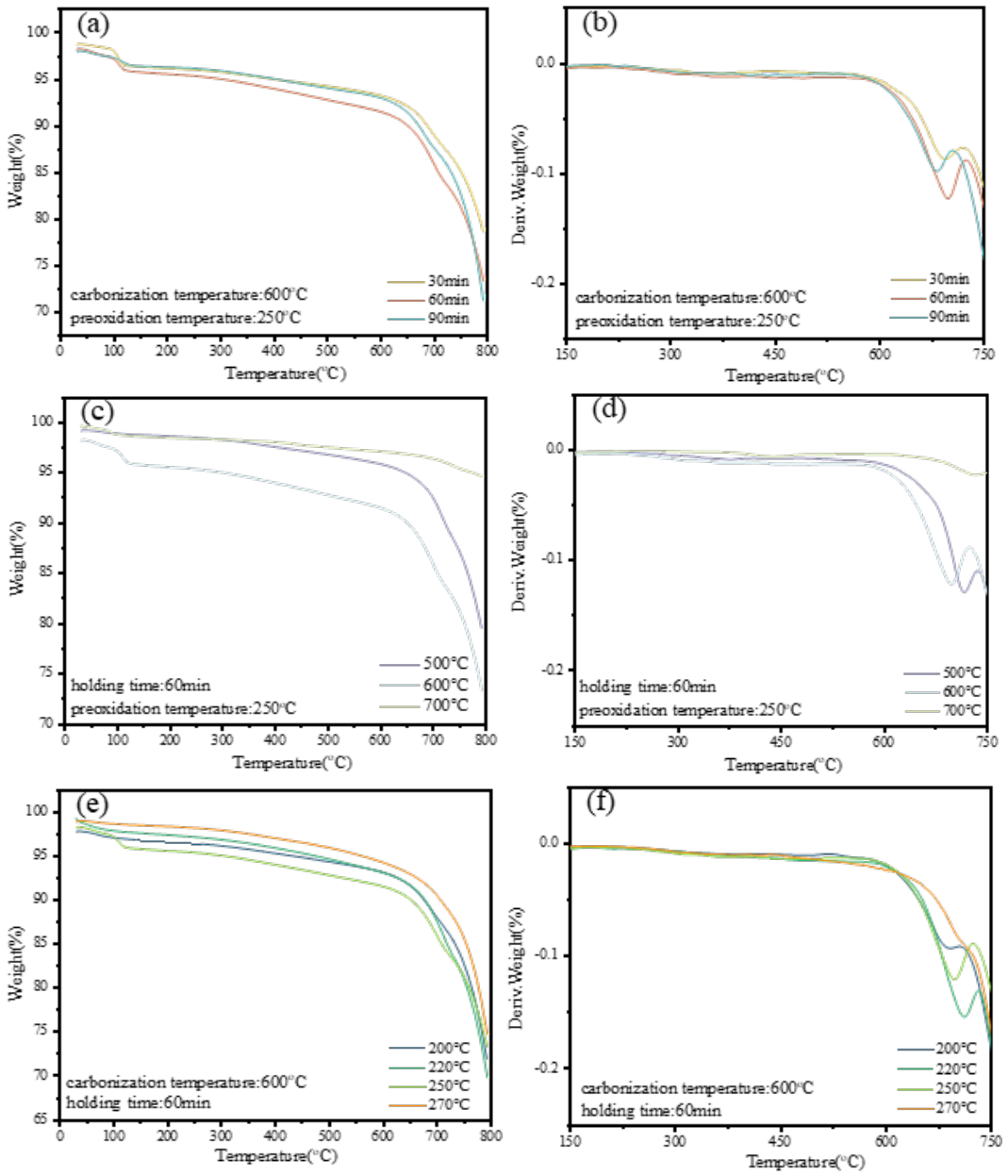

Fig. 9. The TG and DTG curves of carbon fiber prepared with different (a)(b) Carbonization holding time, (c)(d) carbonization temperatures, (e)(f) preoxidation temperatures.

3.3.2. Effect of preoxidation temperature on fiber carbonization results

In Figure 10 (a), the fiber surface is completely melted, indicating that a temperature of 200°C is too low for complete pre-oxidation. On the other hand, in (d), a high pre-oxidation temperature leads to structural defects such as cracks in the fiber. Therefore, both too low and too high pre-oxidation temperatures have a significant adverse effect on maintaining the original fiber structure during carbonization. In (b), partial melting of the fiber is observed, but the fiber structure after carbonization is still mostly intact at a temperature of 250°C.

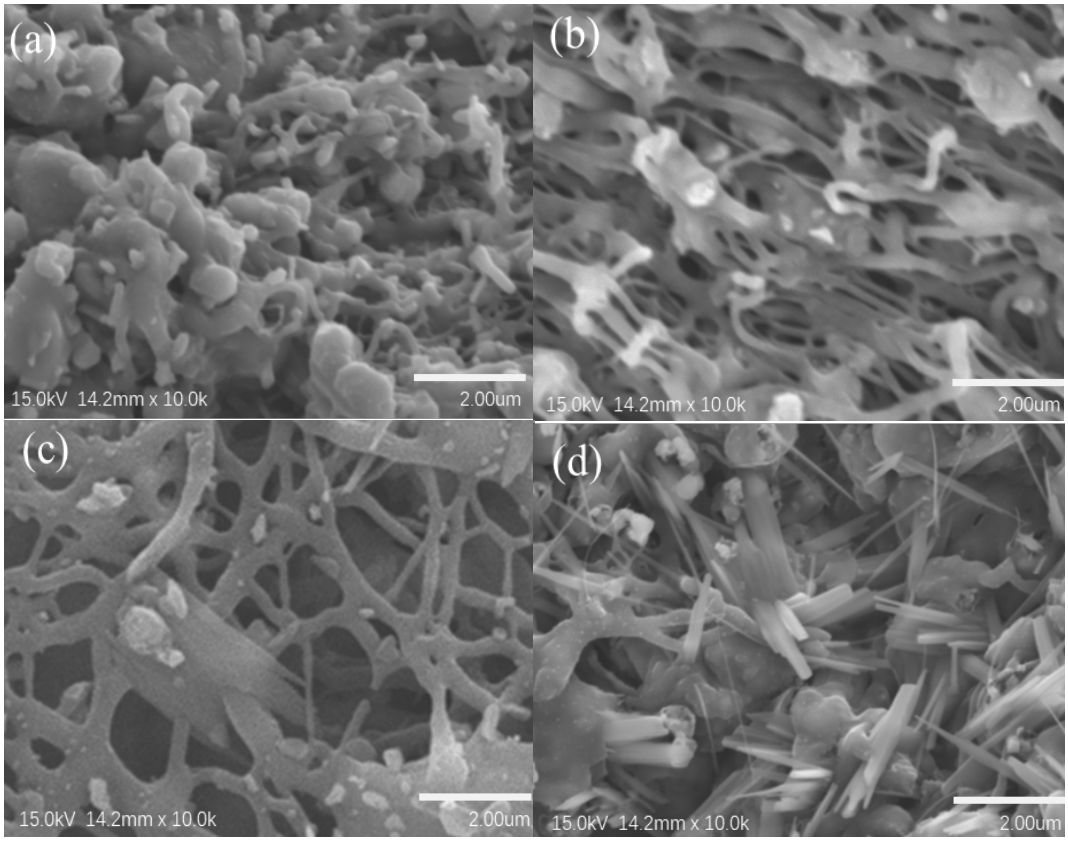

Fig. 10. SEM images of carbon fiber prepared at different (a) preoxidation temperatures 200℃ (b)220℃, (c)250℃, (d)270℃.

3.3.3. Effect of carbonization temperature on fiber carbonization results

In Figure 11 (a), although the fiber structure is well-preserved, there are a significant amount of oxygen-containing impurities on the surface. Combining with (b), it can be observed that the amount of oxygen-containing impurities decreases significantly when the temperature is increased from 500°C to 600°C. In the thermal performance test, the fiber shows a high decomposition rate around 450°C, which is likely due to the decomposition of oxygen-containing impurities. The slower heating rate may have prevented complete decomposition at 500°C. In Figure 3.12 (c), due to the poor thermal stability of pure lignin fibers, complete melting and vaporization occur at a carbonization temperature of 700°C.

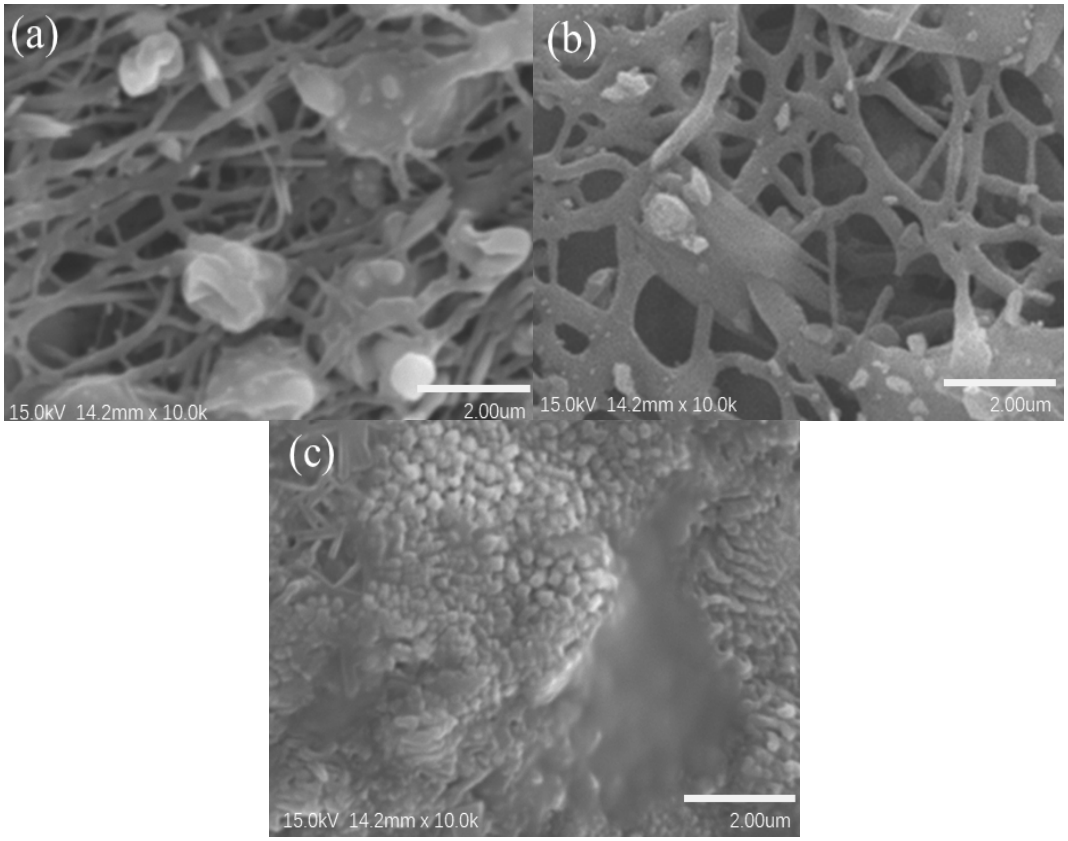

Fig. 11. SEM images of carbon fiber prepared at different carbonization temperatures (a)500℃, (b)600℃, (c)700℃.

3.3.4. Effect of carbonization holding time on fiber carbonization results

Figure 12 (a) shows that a too short insulation time results in a high amount of oxygen-containing impurities remaining. On the other hand, in (c), a too long insulation time leads to fiber melting. A insulation time of about 60 minutes is more suitable, allowing the fiber to decompose oxygen-containing impurities while maintaining its morphology.

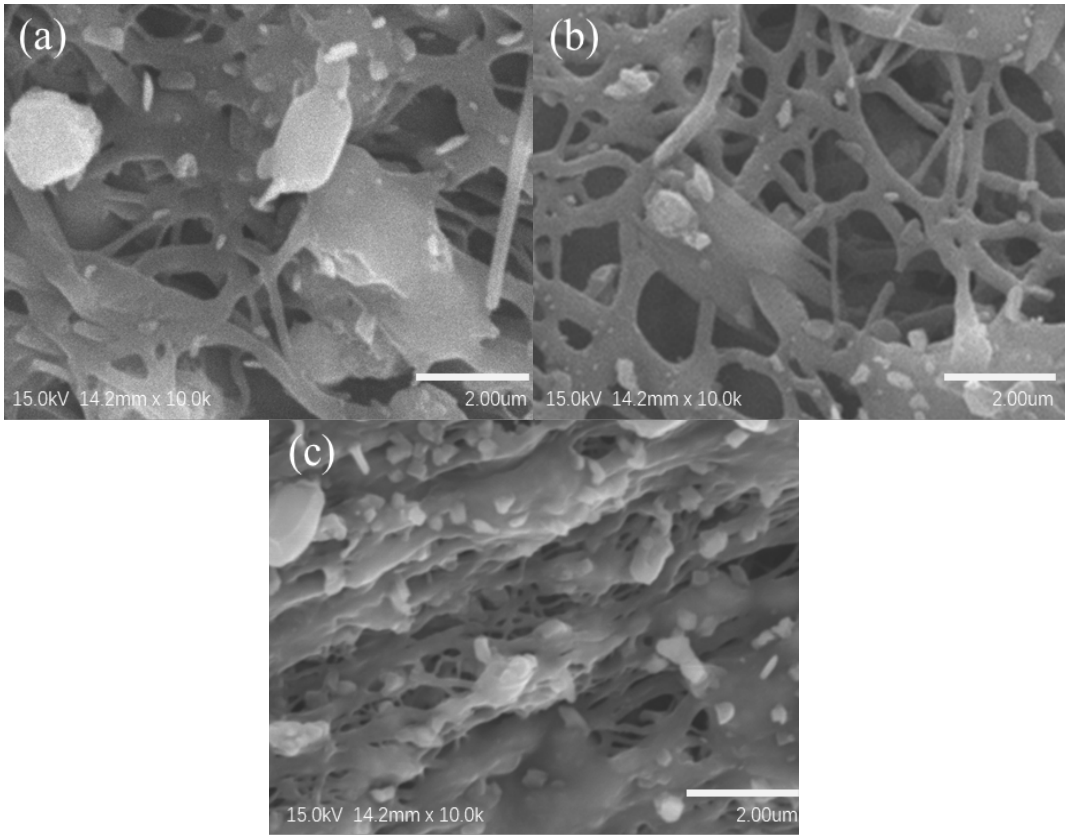

Fig. 12. SEM images of carbon fiber prepared at different carbonization holding time (a)30min, (b)60min, (c)90min.

4. Conclusion

In this study, low-cost carbon fibers were prepared through the electrospinning-pre-oxidation-carbonization route using a green solvent- acetic acid, and a low molecular weight lignin of 500 g/mol with the assistance of PEO. The surface morphology and thermal properties during the preparation process were investigated. It was demonstrated that, under suitable process parameters, carbon fibers can be produced from industrially available low molecular weight lignin, reducing costs and contributing to environmental protection. However, the preparation of carbon fibers from pure low molecular weight lignin requires stringent process parameters and is prone to melting. Slight variations in fiber structure, pre-oxidation temperature, and carbonization temperature can significantly affect the preservation of fiber morphology.

Acknowledgements

The authors are thankful to the support of the Natural Science Foundation of Zhejiang Province (Grant No. LTGS23C160001), the “Pioneer” and “Leading Goose” R&D Program of Zhejiang (Grant No .2022C01066, 2023C01195), and the Fundamental Research Funds for Zhejiang University of Science and Technology (Grant No. 2023QN048, 2023JLZD006).

References

[1] Baker. D. A, Rials. T. G, Journal of Applied Polymer Science 130(2), 713-728 (2013); https://doi.org/10.1002/app.39273

[2] Xu. X, International Journal of Analytical Chemistry 2022 2323534 (2022); https://doi.org/10.1155/2022/7739734

[3] Wang. X, Pan. L, Zheng. A, Bioactive Materials 24 236-250 (2023); https://doi.org/10.1016/j.bioactmat.2022.12.016

[4] Bachmann. J, Hidalgo. C, Bricout. S, Science China Technological Sciences 60(9), 1301-1317 (2017); https://doi.org/10.1007/s11431-016-9094-y

[5] Le. N-D, Trogen. M, Ma. Y, Carbohydrate Polymers 250 116918 (2020); https://doi.org/10.1016/j.carbpol.2020.116918

[6] Tolbert. A, Akinosho. H, Khunsupat. R, Biofuels, Bioproducts and Biorefining 8(6), 836-856 (2014); https://doi.org/10.1002/bbb.1500

[7] Li. Q, Serem. W. K, Dai. W, Journal of Materials Chemistry A 5(25), 12740-12746 (2017); https://doi.org/10.1039/C7TA01187C

[8] Wang. S, Li. Y, Xiang. H, Composites Science and Technology 119 20-25 (2015); https://doi.org/10.1016/j.compscitech.2015.09.021

[9] Jia. G, Zhou. Z, Wang. Q, International Journal of Biological Macromolecules 216 388-396 (2022); https://doi.org/10.1016/j.ijbiomac.2022.06.191

[10] Trogen. M, Le. N-D, Sawada. D, Carbohydrate Polymers 252 117133 (2021); https://doi.org/10.1016/j.carbpol.2020.117133

[11] Chen. J, Ghosh. T, Tang. T, Polymer Engineering & Science 62(4), 1256-1268 (2022); https://doi.org/10.1002/pen.25923

[12] Shi. X, Dai. Z, Cao. Q, New Journal of Chemistry 43(47), 18868-18875 (2019); https://doi.org/10.1039/C9NJ04942H

[13] Zhu. M, Liu. H, Cao. Q, ACS Sustainable Chemistry & Engineering 8(34), 12831-12841 (2020); https://doi.org/10.1021/acssuschemeng.0c03062

[14] Jin. J, Ding. J, Klett. A, ACS Sustainable Chemistry & Engineering 6(11), 14135-14142 (2018); https://doi.org/10.1021/acssuschemeng.8b02697

[15] Li. Q, Xie. S, Serem. W K, Green Chemistry 19(7), 1628-1634 (2017); https://doi.org/10.1039/C6GC03555H